Reverse engineering of spiral bevel gear drives reconstructed from point clouds

Ignacio Gonzalez-Perez[a,*], Alfonso Fuentes-Aznar[b]

[a] *Department of Mechanical Engineering, Materials and Manufacturing, Universidad Politécnica de Cartagena, Spain*

[b] *Department of Mechanical Engineering, Rochester Institute of Technology, USA*

Abstract

The replacement of spiral bevel gears represents a challenge when the design data is missing and only the physical gears are available. In this case, application of reverse engineering is required to determine the design data and machine-tool settings that would allow the default gears to be replaced and/or improved. This paper proposes a methodology of reverse engineering of spiral bevel gears reconstructed from point clouds. Point clouds of the gear tooth surfaces are obtained from non-contact metrology machines using a 3D laser scanner. Non-uniform rational B-splines surfaces are obtained to fit a set of predefined points of the point cloud. Once the reconstructed tooth surfaces are available, a bound-constrained optimization algorithm is used to derive the finishing machine-tool settings of the gears to produce the closer tooth surfaces to the reconstructed ones. The resulting reconstructed gear drive can be analyzed throughout tooth contact and finite element analyses to evaluate its mechanical performance and improve it if necessary. A numerical example, comprising a given design of a face-milled spiral bevel gear drive and the corresponding manufactured gears, shows the advantages and disadvantages of the proposed procedure to capture the designer's intent and analyze the existing gear drive.

Key words: reverse engineering, point cloud, spiral bevel gears, tooth contact analysis, stress analysis

1. Introduction

Reverse engineering constitutes a common practice in the industry to replace or improve default parts whose design is unknown. A comprehensive review of the different issues involved in the technology of reverse engineering, from data acquisition methods to procedures for the conversion of discrete data into a continuous model, can be found in [1]. In the area of gears, a procedure to fit measured gear cutters by means of cubic splines was proposed in [2]. In [3], an alternative equation of meshing was used to facilitate the reverse engineering process of worm gear tooth surfaces. Reverse engineering techniques were also applied in [4] for the modelling of lapping and the prediction of tooth contact results in lapped hypoid gears. In [5], a methodology to reverse engineering of a spiral bevel pinion was proposed starting from the pinion tooth surface data and

*Corresponding author

Email address: ignacio.gonzalez@upct.es (Ignacio Gonzalez-Perez)

tooth contact analysis results. In [6], a zerol spiral bevel pinion was reconstructed adjusting the virtual generated tooth surface to the measured one. In all these works, the data acquisition method was based on the use of a coordinate measuring machine (contact technology). A summary of the advantages of this technology using the mentioned method of data acquisition can be read in [7] where a numerical example to replicate a spiral bevel pinion is presented.

In the last decade, an emerging technology based on the use of non-contact metrology machines has appeared in the market, basically based on the use of optical devices. This technology is able to provide a huge amount of point data, providing a wealth of information not only to assess the quality of the gears but also to perform tooth contact analysis. In [8], new modelling and measuring principles enabling an optical inspection of gears were described in order to catch up all the new income of gear tooth surface information in the metrology analysis. In [9], a comparison between the traditional gear quality assessment based on the use of coordinate measuring machines and the new emerging technology was presented, proposing new parameters to obtain the deviations of the 3D scanned tooth surfaces respect to the nominal tooth surfaces. On the other hand, this new income of gear tooth surface information has required the use of algorithms to manage the point clouds and to get a continuous model. In [10], a K-means clustering algorithm was applied to reverse engineering of a scanned spur gear. In [11], a loaded tooth contact analysis was carried out on two scanned helical gears in mesh with a master gear. Here, a Kd-tree algorithm was considered to reconstruct the tooth surfaces of one pinion tooth. Later, in [12], a scanned helical gear was reconstructed considering the point clouds of all the teeth and the results of application of loaded tooth contact analysis of the to-be-inspected gear in mesh with a master gear presented. In [11, 12], the need to filter the point clouds was revealed due to the inaccuracy of the inspected contact patterns and unloaded functions of transmission errors. Later, in [13], a bilateral filter was applied to the point clouds of a spiral bevel gear tooth before reconstructing the tooth surfaces. The filtering process of the point cloud improves the results of the unloaded tooth contact analysis. However, the contact pressures on the reconstructed tooth surfaces are still overestimated. In order to advance the reverse engineering technique of spiral bevel gear drives, a procedure to determine the finishing machine-tool settings that allow virtually-generated gear tooth surfaces to approach the reconstructed ones is proposed here. In this way, the designer's intent is expected to be caught and the existing gear drive analyzed without overestimating the contact pressures.

A numerical example will be presented where the design of a face-milled spiral bevel gear drive is known. Both face-milled spiral bevel gears are manufactured in a Phoenix II 275G machine according to the provided design. Pinion and gear are scanned later in a HNC3030 non-contact metrology machine. After the tooth surfaces are reconstructed, an algorithm to adjust the basic machine-tool settings allows the virtual generated tooth surfaces to approach the reconstructed ones. Stress analyses of the original design and the design obtained through the reverse engineering approach are performed and the results obtained presented and compared.

2. Reconstruction of spiral bevel gear tooth surfaces from their point clouds

The procedure of reconstruction of a spiral bevel gear starts with the acquisition of point clouds of the tooth surfaces. Here, a non-contact metrology machine based on a 3D laser scanner is considered. Then, the reconstruction of the tooth surfaces is accomplished throughout the following steps (see [13]):

1 Localization of the pitch cone apex.

2 Cleaning and filtering of the point clouds.

3 Obtention of a radial projection of the points and insertion of the flank edges in the radial projection.

4 Computation of a regular grid of points on the radial projection and finding the cloud points that are close to the regular grid points. A Kd-tree algorithm is applied here to perform this task [14].

5 Regeneration of the active and fillet tooth surfaces throughout the application of B-spline surfaces and Hermite curves, respectively. B-spline surfaces [15] are constructed considering the closest points to the regular grid as control points. Hermite curves are considered to approach the to-be-constructed fillet surface to the few points usually available at the fillet.

All these steps are described in detail in [13] and will not be repeated here. The process starts with the localization of the pitch cone apex that represents the origin of the coordinate system in which the coordinates of the cloud points are transformed and considered. Localization of the pitch cone apex requires knowing the value of the mounting distance of the gear and having the scanned points of the back side of the gear. In case this data is not available, the user should adjust the position of the reconstructed gear by trial and error for tooth contact analysis. Figure 1 summarizes the reconstruction of a face-milled spiral bevel pinion from the point clouds of one tooth.

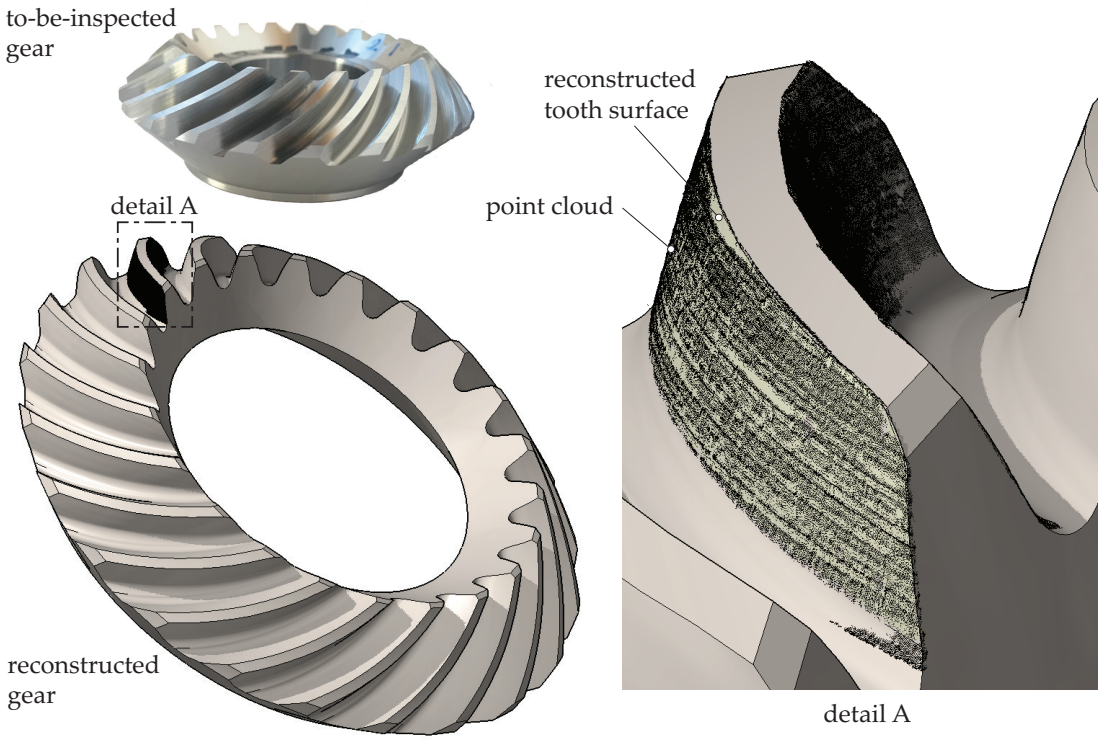

Figure 1: Reconstruction of a spiral bevel pinion (see details in [13]).

3. Derivation of basic gear data and approximate values of finishing machine-tool settings

Once the reconstructed tooth surfaces have been obtained, a procedure to derive basic gear data and to estimate initial values of the finishing machine-tool settings is required. The goal of this procedure is to provide initial values for the machine-tool settings to facilitate the convergence of the optimization algorithm that provides the machine-tool settings producing the closest manufacturable spiral bevel gear tooth surface.

From the visual inspection of the gear drive, the number of teeth of pinion and gear, N_1 and N_2, can be obtained. The proposed methodology is valid for face-milled spiral bevel gear drives with a shaft angle that is considered as known. Therefore, the pitch angles of both gears, γ_1 and γ_2, can be derived according to ANSI/AGMA 2005-C96 [16].

Some basic gear data can be derived from the drawings of the flank edges on the radial projection of the point cloud during the reconstruction of the gear tooth surfaces from the point clouds. Figure 2 shows the radial projection of the point cloud for one of the tooth sides of a gear. The flank edges are drawn by the user by following the boundaries of the radial projection. The pitch angles γ_g, $g = \{1, 2\}$, and the pitch apex locations, are assumed to be known. A coordinate system S_g with its origin O_g located at the pitch apex is considered. The following relations

$$\overline{O_g P_f} = \frac{x_g^{(B)} y_g^{(A)} - x_g^{(A)} y_g^{(B)}}{(x_g^{(B)} - x_g^{(A)}) \sin\gamma_i + (y_g^{(B)} - y_g^{(A)}) \cos\gamma_i} \tag{1}$$

$$\overline{O_g P_b} = \frac{x_g^{(D)} y_g^{(C)} - x_g^{(C)} y_g^{(D)}}{(x_g^{(D)} - x_g^{(C)}) \sin\gamma_i + (y_g^{(D)} - y_g^{(C)}) \cos\gamma_i} \tag{2}$$

allow distances $\overline{O_g P_f}$ and $\overline{O_g P_b}$ to be determined and with them, some basic gear data to be derived as shown below. Here, points A, B, C, and D are obtained at the intersection of the flank edges as shown in Figure 2. The following basic gear data can now be derived:

- The outer pitch cone distance $A_o = \overline{O_g P_b}$.
- The pitch diameter $d_g = 2A_o \sin\gamma_g$, $g = \{1, 2\}$.
- The outer transverse module $m_{ot} = d_g / N_g$, $g = \{1, 2\}$.
- The face width $F_w = \overline{O_g P_b} - \overline{O_g P_f}$.
- The mean cone distance $A_m = A_o - F_w/2$.
- The outer addendum $a_{og} = \overline{P_b C}$.
- The outer dedendum $b_{og} = \overline{D P_b}$.
- The face cone angle can be obtained as

$$\gamma_{Fg} = \arccos\left(\frac{x_g^{(A)} - x_g^{(C)}}{\sqrt{\left(x_g^{(C)} - x_g^{(A)}\right)^2 + \left(y_g^{(C)} - y_g^{(A)}\right)^2}} \right) \tag{3}$$

- The root cone angle can be obtained as

$$\gamma_{Rg} = \arccos\left(\frac{x_g^{(B)} - x_g^{(D)}}{\sqrt{\left(x_g^{(D)} - x_g^{(B)}\right)^2 + \left(y_g^{(D)} - y_g^{(B)}\right)^2}}\right) \tag{4}$$

- The mean addendum $a_{mg} = a_{og} - F_w \tan(\gamma_{Fg} - \gamma_g)/2$.
- The mean dedendum $b_{mg} = b_{og} - F_w \tan(\gamma_g - \gamma_{Rg})/2$.

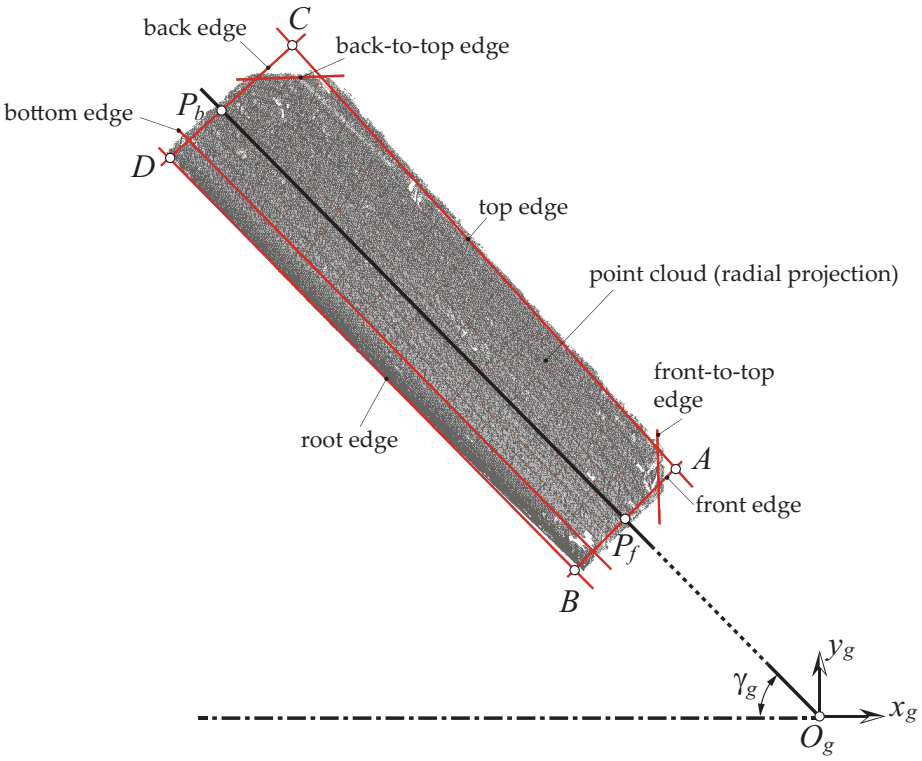

Figure 2: For the determination of some basic gear data from the radial projection of the point cloud.

After reconstruction of both sides of the gear tooth surfaces from the point clouds, further basic gear data and initial values of the finishing machine-tool settings are derived as described below (see Fig. 3):

(1) Intersection curves between the pitch cone and the reconstructed tooth surfaces are obtained. These curves (named as helix curves) cover from point H_{lf} to point H_{lb} for the left side curve, and from point H_{rf} to point H_{rb} for the right side curve (see detail A in Fig. 3).

(2) Points M_l and M_r are determined as those points on the helix curves that are at a mean cone distance A_m from the pitch apex O_g.

(3) Point O_m is obtained on the gear axis and it is located at a distance $A_m \cos\gamma_g$ from the pitch apex O_g.

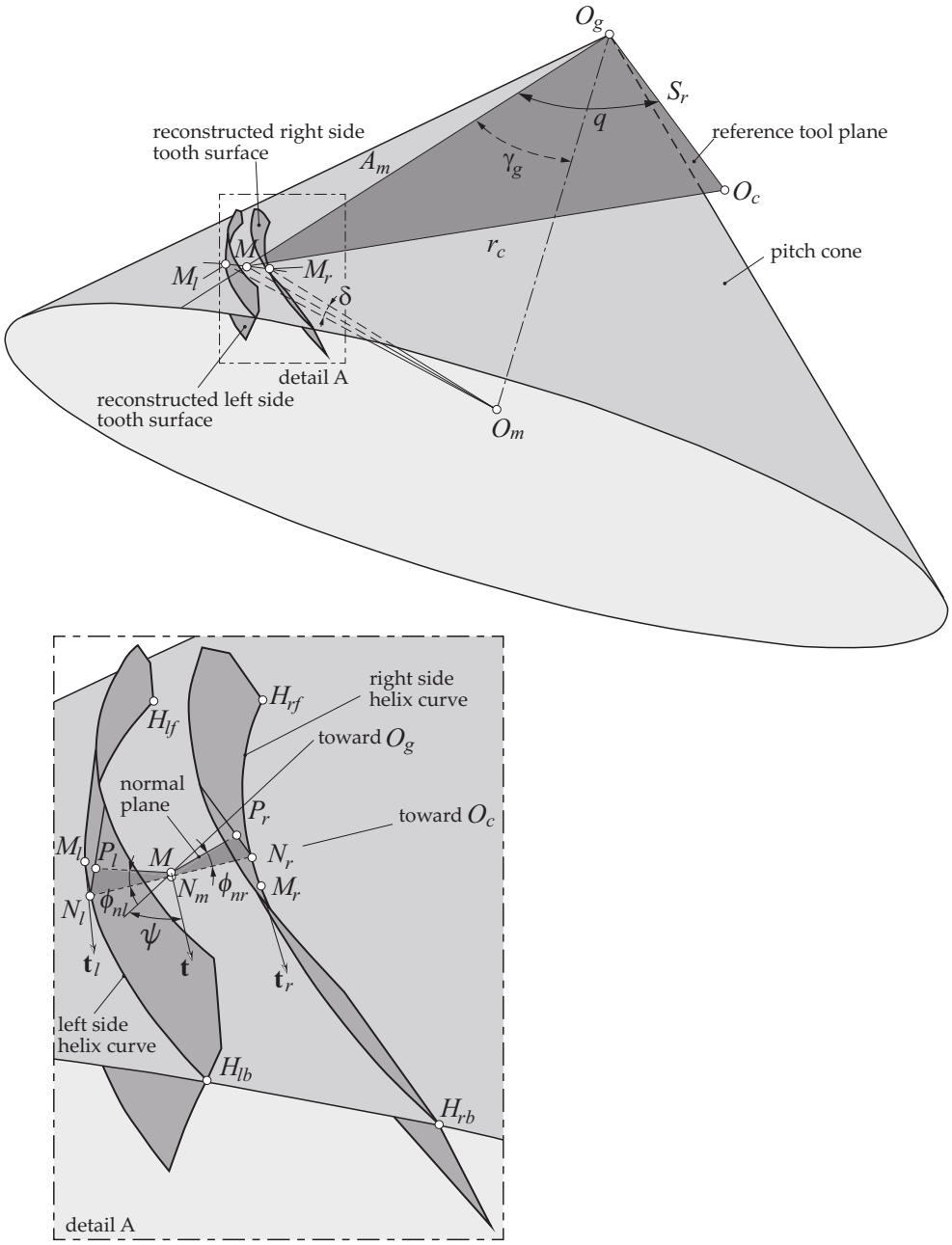

Figure 3: For the estimation of further basic gear data and initial values of the finishing machine-tool settings.

(4) Point M is obtained on the pitch cone by rotation of points M_l or M_r around $\overline{O_g O_m}$ in the plane defined by the three points M_l, M_r, and O_m. The rotation angle is half of the angular tooth space defined by the three mentioned points (angle δ in Fig. 3).

(5) The tangents to the left and right helix curves are evaluated at points M_l and M_r, respectively, as $\mathbf{t}_l$ and $\mathbf{t}_r$. Then, the tangent at point M is evaluated as $\mathbf{t} = (\mathbf{t}_l + \mathbf{t}_r)/2$.

(6) The spiral angle ψ (see detail A in Fig. 3) is evaluated as

$$\psi = \arccos\left(\frac{\overrightarrow{O_g M}\cdot\mathbf{t}}{\overline{OgM}}\right) \tag{5}$$

(7) A plane that passes through point M and whose normal is parallel to vector $\mathbf{t}$ allows points N_l and N_r to be found on the helix curves. Such a plane will be considered as the normal plane.

(8) Intersection curves between the reconstructed tooth surfaces and the normal plane allows points P_l and P_r to be found as those points whose tangents are perpendicular to vectors $\overrightarrow{MP_l}$ and $\overrightarrow{MP_r}$, respectively.

(9) An intermediate point N_m is determined as the midpoint from points N_l and N_r.

(10) The normal chordal tooth thickness can be evaluated as $t_{ng} = \overline{N_l N_r}$.

(11) The normal chordal addendum can be evaluated as $a_{cg} = a_{mg} + \overline{MN_m}$.

(12) The normal pressure angles ϕ_{nl} and ϕ_{nr} are evaluated as (see detail A in Fig. 3)

$$\phi_{nl} = \arccos\left(\frac{\overrightarrow{N_m N_l}\cdot\overrightarrow{MP_l}}{\overline{N_m N_l}\cdot\overline{MP_l}}\right) \tag{6}$$

$$\phi_{nr} = \arccos\left(\frac{\overrightarrow{N_m N_r}\cdot\overrightarrow{MP_r}}{\overline{N_m N_r}\cdot\overline{MP_r}}\right) \tag{7}$$

(13) The curvatures of the helix curves at the points N_l and N_r are estimated as (see [17]):

$$\kappa_l = \frac{\left|\mathbf{r}_\theta^{(N_l)}\times\mathbf{r}_{\theta\theta}^{(N_l)}\right|}{\left|\mathbf{r}_\theta^{(N_l)}\right|^3} \qquad \kappa_r = \frac{\left|\mathbf{r}_\theta^{(N_r)}\times\mathbf{r}_{\theta\theta}^{(N_r)}\right|}{\left|\mathbf{r}_\theta^{(N_r)}\right|^3} \tag{8}$$

Here, θ represents the curve parameter. The first and second derivatives, $\mathbf{r}_\theta$ and $\mathbf{r}_{\theta\theta}$, can be estimated numerically through central difference approximations with an error of order $\Delta\theta^4$ (see [18]) or by using the analytical form of the B-Spline reconstructed surface.

(14) The cutter radius r_c (see Fig. 3) can be estimated as

$$r_c \approx \frac{1}{2}\left(\frac{1}{\kappa_l}+\frac{1}{\kappa_r}\right) \tag{9}$$

(15) The radial distance and cradle angle can be estimated from the construction of the reference tool plane (see Fig. 3) as

$$S_r \approx \sqrt{A_m^2 + r_c^2 - 2A_m r_c \sin\psi} \tag{10}$$

$$q \approx \arcsin\left(\frac{r_c}{S_r}\cos\psi\right) \tag{11}$$

Here, for the construction of the reference tool plane, the distance $\overline{N_m M}$ is considered as negligible.

(16) The velocity ratio is the quotient of the velocity of the gear and the velocity of the cradle in the generation process and can be estimated as

$$m_{gc} = \frac{\omega_g}{\omega_c} \approx \frac{A_m}{\overline{O_m M}} \tag{12}$$

(17) The pressure angles α_{bl} and α_{br} of the blades of the cutter depend on the inclination of the tool plane with respect to the reference tool plane displayed in Fig. 3 in order to guarantee the normal pressure angles ϕ_{nl} and ϕ_{nr} of the tooth. Usually, the tool plane contains a generatrix of the root cone (not shown in Fig.3), whereas the reference tool plane illustrated in Fig. 3 contains a generatrix of the pitch cone (from O_g to M). It is assumed that the pressure angles of the blade will be closer to the normal pressure angles derived through Eqs. (6) and (7), so these values will work as initial values of the blade pressure angles in the optimization process.

4. Optimization process to adjust the finishing machine tool settings

Once the reconstructed tooth surfaces have been obtained and some basic gear data and approximate values of basic machine-tool settings have been derived, the adjustment of the finishing machine-tool settings has to be carried out. This adjustment is performed by minimizing the deviations between a manufacturable gear surface and the reconstructed one. This process is based on the application of the Levenberg−Marquardt (LM) algorithm [19, 20]. The LM algorithm is used in nonlinearly bound constrained and unconstrained optimization problems in which the objective function is formulated in terms of least-squares. In our case, the objective function is of the type $f(\mathbf{x}) : R^n \rightarrow R$. Here, $\mathbf{x}$ is a vector of dimension n where n is the number of independent variables, corresponding to those finishing machine-tool settings and cutter parameters that allow a virtually generated tooth surface to become the closer surface to the reconstructed one. Function $f(\mathbf{x})$ is defined as a sum of the squares of m functions $d_j(\mathbf{x}) : R^n \rightarrow R$, $j = \{1, \ldots, m\}$ with $m > n$. Here, $d_j(\mathbf{x})$ is defined as the distance between the virtually generated tooth surface and the reconstructed one at a grid point j of the former surface. This algorithm has been chosen since it can handle suitably the possible dependencies among the machine-tool settings and the existence of high non-linearity between them and the deviations of the tooth surfaces.

The optimization algorithm considers as objective surface the reconstructed one. The virtually generated tooth surface is defined as a function of a set of independent variables (see [17] for a better understanding of these variables that define the cutter geometry, the position of the cutter relative to the gear blank, and the relative cutting motion between both parts):

- The machine center to back, ΔX_D.
- The sliding base, ΔX_B.
- The blank offset, ΔE_m.
- The radial distance, S_r.
- The cradle angle, q.
- The machine root angle, γ_m.

- The swivel and tilt angles, j and i.
- The velocity ratio or ratio of gear roll, m_{gc}, $g = \{1, 2\}$.
- The modified roll coefficients C and D.
- The cutter point radius, R_g.
- The root fillet radius, ρ_f.
- The parabola coefficient a_p for profile crowning.
- The location of the point of tangency of such a parabola with the straight reference profile, u_0.
- The blade pressure angle, α_b.

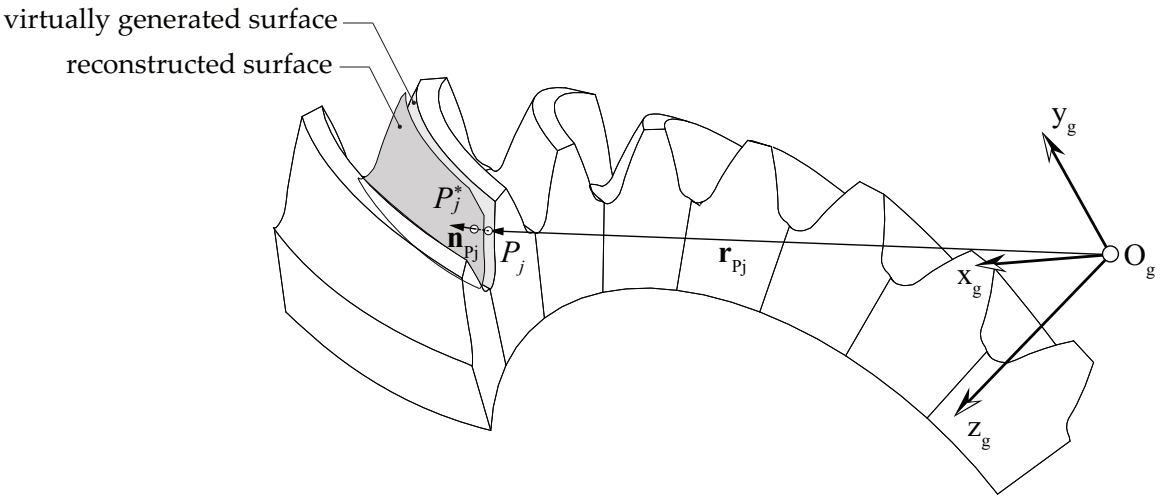

Figure 4: Schematic representation of the objective surface (the reconstructed one) and the virtually generated tooth surface.

Distance $d_j(\mathbf{x})$ is defined as (see Fig. 4)

$$d_j(\mathbf{x}) = [\mathbf{r}_{P_j^*} - \mathbf{r}_{P_j}(\mathbf{x})] \cdot \mathbf{n}_{P_j}(\mathbf{x}) \tag{13}$$

Here, P_j, $j = \{1, \ldots, m\}$, is any point from a grid of m points defined on the virtually generated tooth surface, and $\mathbf{x} = \{S_r\ ,\ q,\ \gamma_m,\ j,\ i,\ \Delta X_B,\ \Delta E_m,\ \Delta X_D,\ m_{gc},\ C,\ D,\ R_g,\ \rho_f,\ a_p,\ u_0,\ \alpha_b\}$. Point P_j^* is the projected point of point P_j on the reconstructed tooth surface. The projection is made along the unit normal $\mathbf{n}_{P_j}$. The vectors $\mathbf{r}_{P_j}$ and $\mathbf{n}_{P_j}$ are evaluated at each point P_j following the theory of gearing [17] and considering the relative motions between the face-milling cutter and the gear blank. Finally, the objective function is defined as

$$f(\mathbf{x}) = \sum_{j=1}^{m} [d_j(\mathbf{x})]^2 \qquad \mathbf{x} \in \Omega \tag{14}$$

Here, Ω represents the domain where the independent variables can exist. Determination of the limit values of the variables x_i, $i = \{1, \ldots, n\}$, is very important for the convergency of the algorithm to a feasible solution. Therefore, the determination of approximate values for finishing machine-tool settings as shown in the previous section is crucial to get adequate limits of the variables around these approximate values.

5. Tooth contact and stress analyses

The tooth contact analysis algorithm is based on an improvement of the work [21] and has been applied later by the authors in several references such as in [13]. It is based on the minimization of the distance between three pairs of contacting tooth surfaces, which are considered as rigid, obtaining the contact pattern after setting a value for the so-called virtual marking compound thickness.

The stress analysis is based on the application of the finite element method through models that have been constructed following the ideas exposed in [22]. The finite element models are based on five pairs of contacting teeth. Two regions of meshing are identified: (i) a refined region with three layers of linear brick elements C3D8I (see [23]) around the contacting surfaces and fillet areas, and (ii) a coarse region with quadratic brick elements C3D20 (see [23]) for the remaining tooth body. Both regions are joined through a tie-surface constraint to guarantee the continuity of the displacements. Figure 5 shows the finite element model considered in this work. The three layers of elements C3D8I have enough thickness to guarantee that the maximum Von Mises stress occurs inside that refined region ($0.24m_{ot}$). The degrees of freedom of pinion and gear are controlled through two reference nodes located on the gear axes. Both nodes are attached to their corresponding rigid surfaces, which are located on the lateral sides and bottom part of the gear rims. A torque T is applied to the pinion reference node while the gear reference node is blocked at each step of the analysis. The number of steps coincides with the number of contact positions used in the tooth contact analysis algorithm.

6. Numerical example

6.1. The given design of a spiral bevel gear drive

The design of a face-milled spiral bevel gear drive is known ahead. Table 1 shows the basic data of the gear drive and Table 2 shows the cutter parameters and finishing machine-tool settings for the concave and convex tooth sides of pinion and gear.

Figure 6(a) shows the contact pattern and the contact path on the concave tooth side of the pinion model for a counterclockwise rotation of the pinion. A virtual marking compound thickness of 0.0065 mm is considered. The function of unloaded transmission errors is also illustrated, showing a maximum peak-to-peak level of 8 arcsec. Similar results are illustrated in Fig. 6(b) for a clockwise rotation of the pinion. In both cases, a longitudinally oriented path of contact is observed.

The given design is based on a longitudinally oriented path of contact to avoid areas of severe contact stresses at the tip of the teeth during the cycle of meshing. This statement can be confirmed with the results of the stress analysis of the gear drive. A pair of finite element models as the one illustrated in Fig. 5 considering clockwise and counterclockwise rotations of the pinion allow the evolution of maximum contact pressure to be obtained and represented for both directions of rotation. The finite element models consider 121300 elements and 174572 nodes. A torque of 197.0 Nm is applied to the pinion whereas the gear is held at rest at each step. Figure 7 shows the

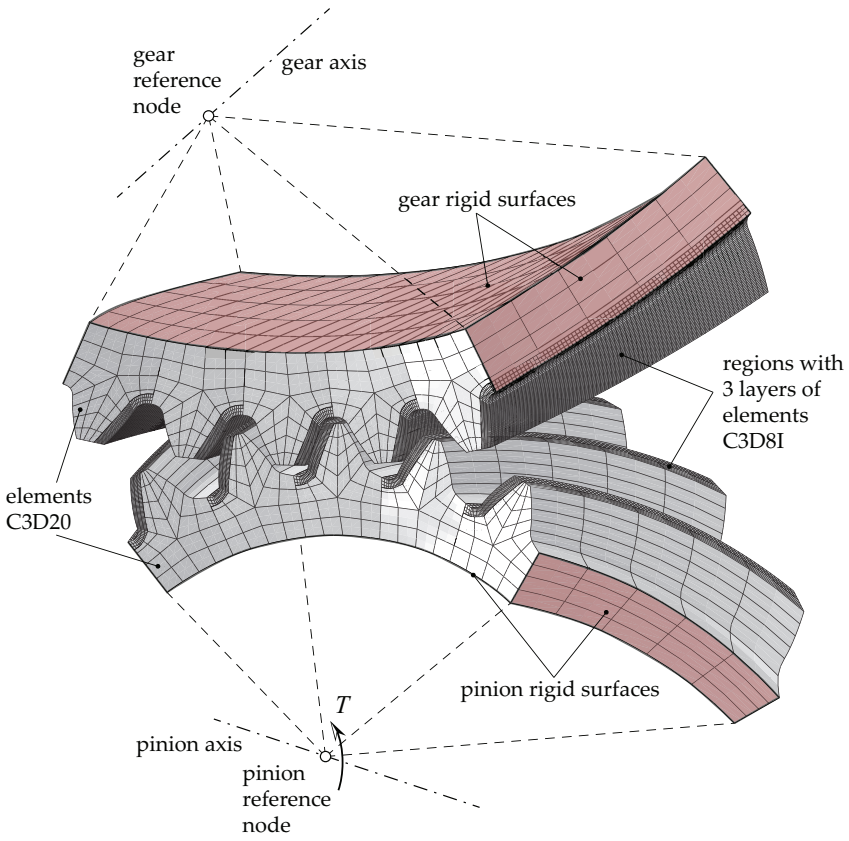

Figure 5: Finite element model of the pinion.

evolution of the contact pressure along a total of 41 steps distributed along two angular pitches of rotation of the pinion.

6.2. The reconstructed spiral bevel gear drive

Both, the pinion and the gear are manufactured in a Phoenix II 275G machine according to the given design (Figure 8) and then scanned in a HNC3030 non-contact metrology machine.

The reconstructed pinion and gear models are obtained following the procedure described in [13]. Firstly, the localizations of the pitch cone apexes, O_1 and O_2, on the pinion and gear axes are determined from the location of the back planes and considering as known the mounting distance (m_d=58.1 mm). Figure 9 shows the reconstructed models of pinion and gear and their corresponding point clouds. Two sets of point clouds are observed at each gear: one corresponds to the back plane, the other set corresponds to both tooth sides of one tooth. The back planes provides the points O_{b1} and O_{b2} on the pinion and gear axes of rotation, respectively. Then, the location of the pitch apexes O_g, $g = \{1, 2\}$, can be easily determined with the provided mounting distance ($\overline{O_{bg}O_g} = m_d$).

After filtering the point clouds of both tooth sides using a bilateral filter with $r = r_n = 100$ μm and $n_{iter} = 3$ (see details in [13]), a grid of 10×15 points has been considered on the radial projection of each filtered point cloud. Each grid is constructed once the flank edges have been laid out by the user on the radial projection of the point cloud (see Fig. 10). The process is repeated twice for each tooth side and for both pinion and gear teeth.

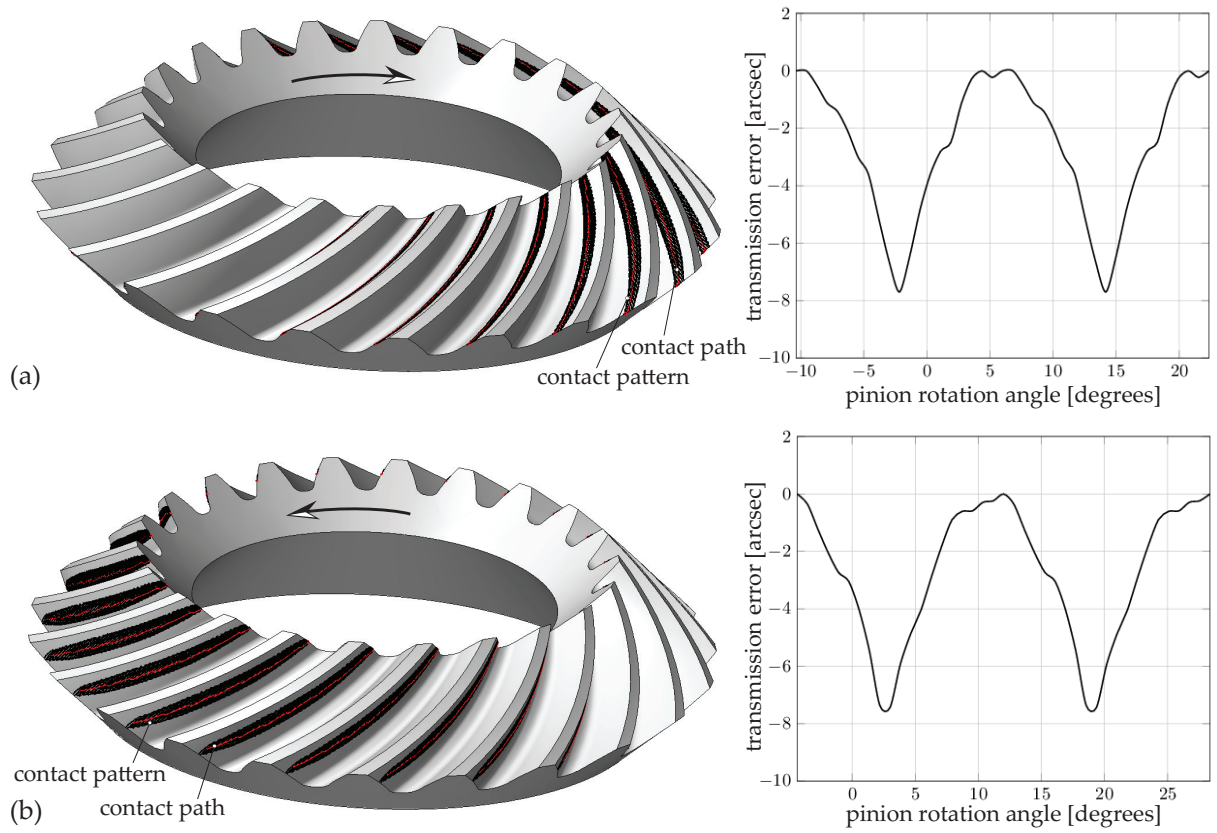

Figure 6: Tooth contact analysis results in the given design for: (a) counterclockwise rotation of the pinion, and (b) clockwise rotation of the pinion.

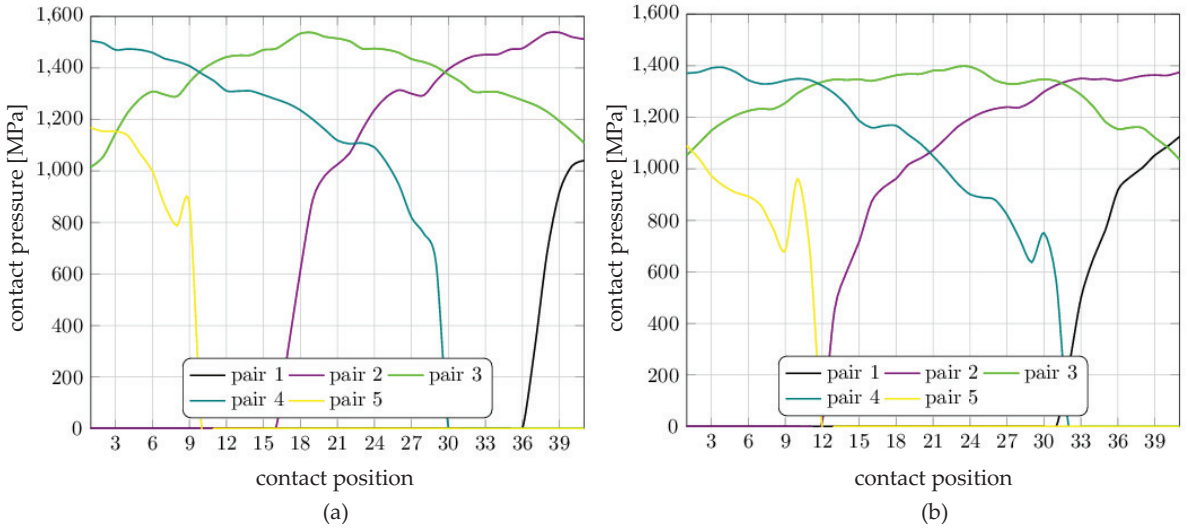

Figure 7: Contact pressure evolution for the given design when the pinion is rotated: (a) counterclockwise (pinion concave - gear convex) and (b) clockwise (pinion convex - gear concave).

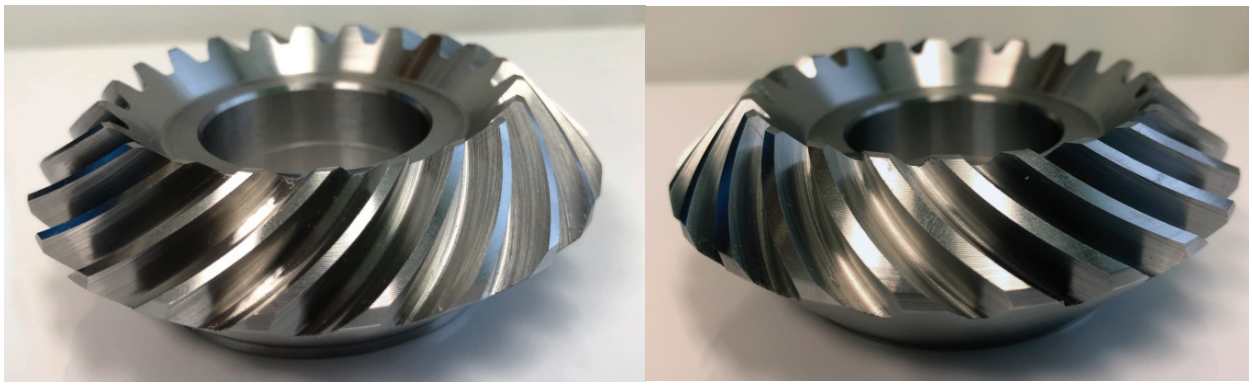

(a) (b)

Figure 8: Manufactured parts of the given design: (a) pinion and (b) gear.

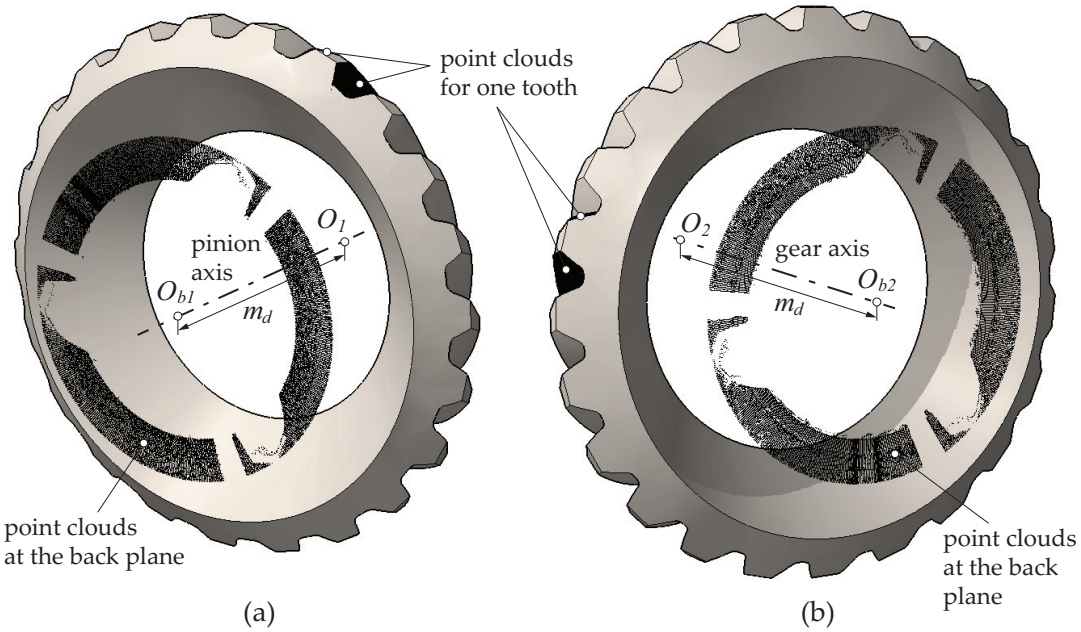

Figure 9: Illustration of the point clouds and the reconstructed models for: (a) pinion and (b) gear.

Table 1: Basic data of the spiral bevel gear drive.

Data	Pinion	Gear
Shaft angle, γ [°]	90.0	
Tooth number, N_g	22	23
Pitch angle, γ_g [°]	43.727	46.273
Spiral angle, ψ [°]	45.0	
Hand of spiral	Right-hand	Left-hand
Outer transverse module, m_{ot} [mm]	3.740	
Face width, F_w [mm]	18.0	
Tooth taper	Duplex	
Outer addendum, a_{og} [mm]	2.823	2.344
Outer dedendum b_{og}[mm]	2.906	3.384
Face cone angle, γ_{Fg} [°]	46.084	48.233
Root cone angle, γ_{Rg} [°]	41.767	43.916
Dedendum angles, δ_g [°]	1.960	2.357

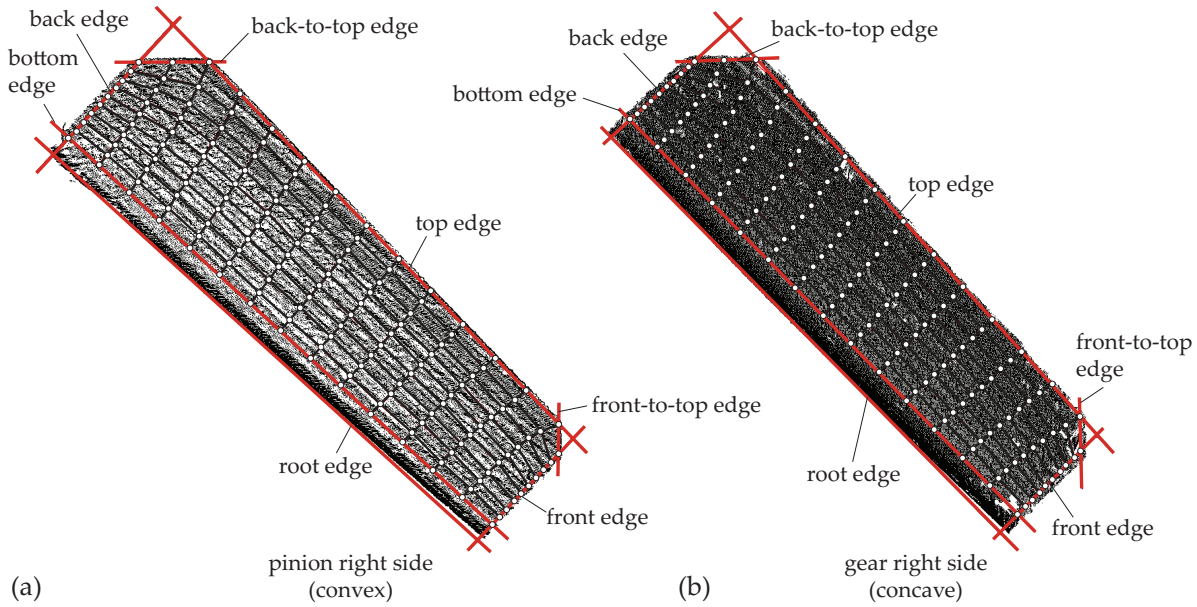

Figure 10: Radial projections of the point clouds with illustration of the flank edges and the corresponding grids for (a) pinion convex tooth side and (b) gear concave tooth side.

Irregularities on the reconstructed tooth surfaces from point clouds, even after application of the filtering process, do not allow the same TCA results as for the theoretical geometry of the given design (Fig. 6) to be obtained. The virtual marking compound thickness to apply TCA on reconstructed tooth surfaces should be increased to at least 0.02 mm. Figure 11 shows the TCA results for the reconstructed pinion rotating in clockwise direction and in mesh with the reconstructed gear. The contact pattern is formed by isolated contact areas in the gear tooth surfaces yielding a function of unloaded transmission errors with a peak-to-peak maximum value of about 140 arcsec. In addition, the stress analysis results of the reconstructed gear drive (see Fig. 12) show high values of contact stresses that are very far from those expected for the given

Table 2: Cutter parameters and finishing machine-tool settings of the given design.

Data	Pinion (CC)	Pinion (CV)	Gear(CC)	Gear(CV)
Cutting method	Face-milling			
Cutter type	Fixed-setting		Spread-blade	
Point radius [mm]	39.725	47.860	45.075	43.825
Blade pressure angle [degrees]	21.644	18.316	18.316	21.644
Blade profile	Parabolic		Straight	
Parabola coef. [mm^{-1}]	0.0008		NA	
Parabola tangency point [mm]	3.031	2.959	NA	
Bottom relief height [mm]	NA		NA	1.5
Bottom relief parabola coef. [mm^{-1}]	NA		NA	0.005
Machine center to back [mm]	-3.512	0.525	0.0	
Sliding base [mm]	1.471	-1.218	-0.932	
Blank offset [mm]	1.218	0.631	0.0	
Radial distance [mm]	32.119	38.194	36.748	
Cradle angle [degrees]	52.454	56.547	58.794	
Machine root angle [degrees]	41.767	41.767	43.916	
Tilt angle [degrees]	0.0	0.0	NA	
Velocity ratio	1.2746	1.4893	1.3826	
Modified roll coef. C	-0.02719	0.01765	NA	
Modified roll coef. D	0.06442	-0.01393	NA	

CC: concave, CV: convex, NA: not applicable

design (see Fig. 7).

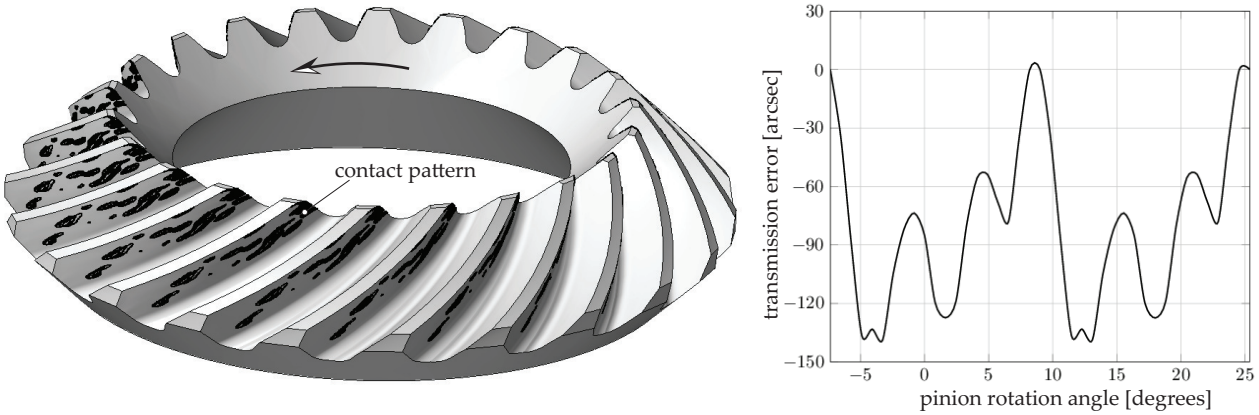

Figure 11: Tooth contact analysis results for the reconstructed gear drive for a clockwise rotation of the pinion.

6.3. Estimation of basic gear data from the reconstructed gears

The tooth number of pinion and gear is known by a visual inspection of the gears. The pitch angles can also be derived following the Standard [16] from the tooth numbers and the shaft angle γ (that is assumed to be known and equal to 90° in this numerical example). Furthermore, following the procedure exposed in Section 3, some basic gear data is derived for the gear and the pinion (see Table 3).

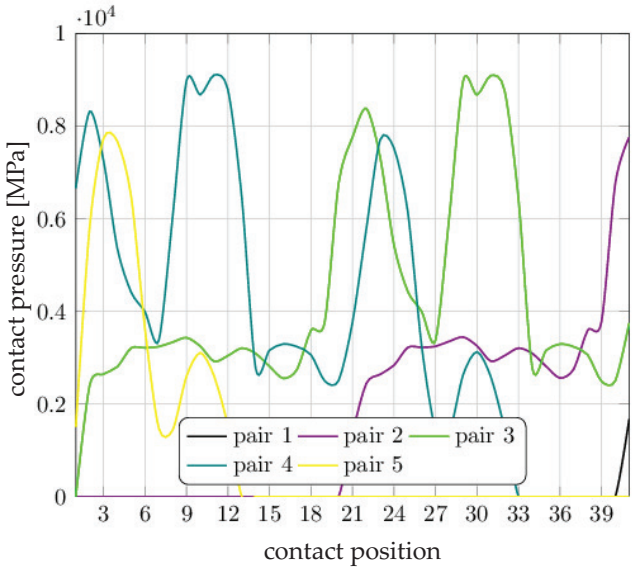

Figure 12: Contact pressure evolution in the reconstructed gear drive when the pinion is rotated clockwise.

Table 3: Estimated basic gear data of the reconstructed spiral bevel gear drive.

Estimated Basic Data	Gear	Pinion
Spiral angle, ψ [°]	44.938	45.118
Face width, F_w [mm]	17.944	17.955
Outer transverse module, m_{ot} [mm]	3.733	3.740
Outer addendum, a_{og} [mm]	2.288	2.751
Outer dedendum, b_{og} [mm]	3.351	2.627
Face cone angle, γ_{Fg} [°]	48.468	46.431
Root cone angle, γ_{Rg} [°]	43.046	41.199
Mean addendum, a_{mg} [mm]	1.944	2.327
Mean dedendum, b_{bg} [mm]	2.845	2.231
Curvature radius, r_c [mm]	40.602	44.696
Normal pressure angle (left side), ϕ_{nl} [°]	19.886	19.973
Normal pressure angle (right side), ϕ_{nr} [°]	20.187	19.361
Normal chordal tooth thickness, t_{ng} [mm]	3.607	3.311
Mean chordal addendum, a_{cg} [mm]	1.950	2.401

Some values of the derived parameters depend on the flank edges traced on the radial projection of the point clouds (see Fig. 10). In this case, it is observed that the derived outer transverse module in the gear (see Table 3) almost matches the outer transverse module of the provided gear drive (see Table 1). The estimation of the outer transverse module allows the user to have an idea of the size of the gear drive and estimate the design torque of the gear drive. The AGMA 2005-C96 Standard [16] allows the pinion torque to be estimated out of the gear ratio N_2/N_1 and the pinion pitch diameter $d_1 = m_{ot}N_1$. For this numerical example, the estimated pinion torque is 197.0 Nm.

On the other hand, the no coincidence of the derived root cone angles (see Table 3) with the pitch angles (see Table 1) allows the user to foresee that a duplex type of taper has been implemented in the gear drive. The difference between the pitch angles and the root cone angles allows the

dedendum angles for the pinion and the gear to be estimated ($\delta_1 = 2.528°$, $\delta_2 = 3.227°$). In this point, we have to say that the poor quality of the point clouds at the fillet areas (as a consequence of the scanning process), the manual location of the root flank edges by the user (see Fig. 10), and the small values of the expected dedendum angles (see Table 1), may produce important errors in the estimation of the dedendum angle from the reconstructed gear. In this case, an alternative measuring method may be more convenient to estimate the root cone angle and therefore the dedendum angle.

6.4. Estimation of the basic machine-tool settings for the gear

A first approach for the estimation of the finishing machine tool settings for the gear has been based on the procedure exposed in Section 3. A second approach is based on the procedure exposed in [24] considering the most general type of taper (the duplex taper) and the expected values of some basic gear data (see Table 3) such as a value of 45.0° for the spiral angle, a value of 18.0 mm for the face width, and the estimated dedendum angle $\delta_2 = 3.227°$. A mean cutter radius of R_u=44.45 mm (1.75 inches) as listed in the AGMA Standard 2005-C96 [16] is the closest one to the estimated curvature radius r_c (see Table 3) and it is being considered in the second approach. Table 4 shows the estimated basic machine-tool settings following the two approaches and the basic machine-tool settings of the given design.

Table 4: Estimated and given basic machine-tool settings of the gear.

Basic Machine-Tool Setting	Approach 1	Approach 2 [24]	Approach 2* [24]	Given Design
Machine center to back, ΔX_{D2} [mm]	NA	0.0	0.0	0.0
Sliding base, ΔX_{B2} [mm]	NA	-0.00024	-0.904	-0.932
Blank offset, ΔE_{m2} [mm]	NA	0.0	0.0	0.0
Radial distance, S_{r2} [mm]	36.044	36.685	36.704	36.748
Cradle angle, q_2 [degrees]	52.883	58.956	58.906	58.794
Machine root angle, γ_{m2} [degrees]	43.046	43.046	43.916	43.916
Velocity ratio, m_{2c}	1.38381	1.38162	1.3826	1.3826

NA: not available; *: with a better estimation of γ_{R2}

The approach 1 does not provide values for some basic machine-tool settings such as ΔX_{D2}, ΔX_{B2}, and ΔE_{m2}. However, the approach 2 considers that a duplex type of taper is implemented in the reconstructed gear drive. Following the procedure described in [24] for this type of taper, a better estimation of the basic machine-tool settings is achieved. However, the sliding base is still far from the objective value due to a bad estimation of the root cone angle γ_{R2} and the dedendum angle δ_2 ($\delta_2 = \gamma_2 - \gamma_{R2}$) since $\Delta X_{B2} = A_m \sin\delta_2 - b_{m2}\cos\delta_2$ (see [24]).

The results from the application of the approach 2 can be improved if a better estimation of the root cone angle γ_{R2} is made. This can be verified in the fourth column of Table 4 where a root cone angle $\gamma_{R2} = 43.916°$ is considered.

Regarding the point width and the blade pressure angles of the gear cutter, an approach similar to the one described in [25] can be applied considering as input data an expected normal pressure angle of 20.0° (see the estimated normal pressure angles for the left and right tooth sides of the gear in Table 3), an estimated normal chordal tooth thickness $t_{n2} = 3.607$ mm, and an estimated mean chordal addendum $a_{c2} = 1.95$ mm.

Figure 13 shows a comparison between the estimated gear tooth surface obtained from the approach 2*, assuming the same values for the cutter blade angles and point width than those of the given design of the gear, and the reconstructed gear tooth surface. The differences are below 1.0 μm for the convex tooth side (left side) and below 2.0 μm for the concave tooth side (right side).

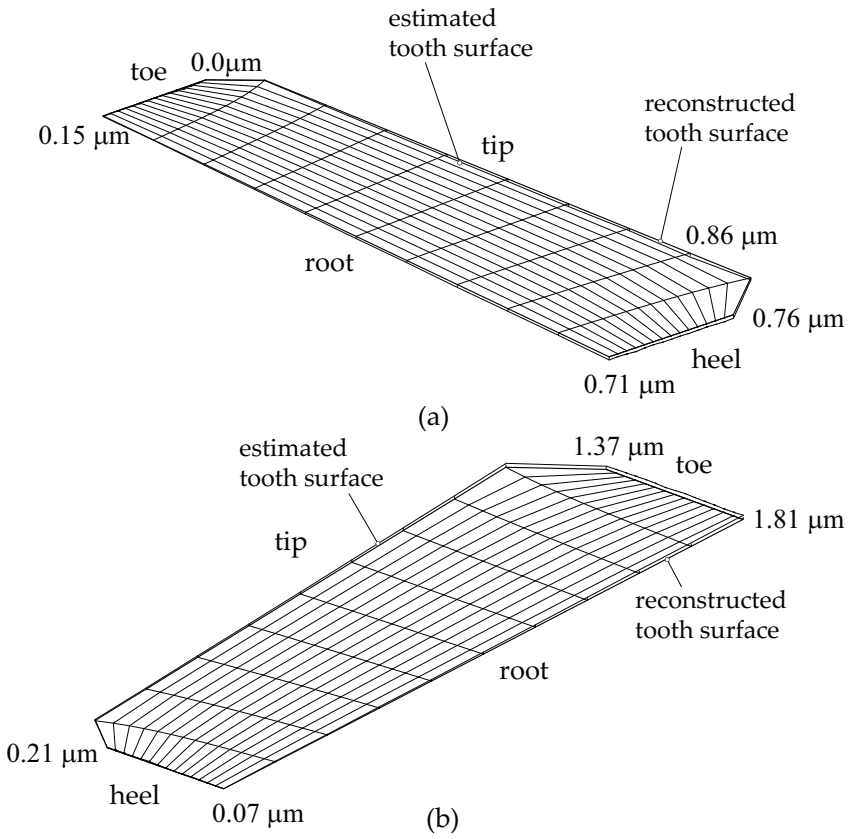

Figure 13: Geometry comparison between the reconstructed gear tooth surfaces and the estimated ones (through the approach 2*) at: (a) the convex tooth side (left side) and (b) the concave tooth side (right side).

6.5. Determination of the basic machine-tool settings of the pinion

Both tooth sides of the pinion are assumed to be generated independently. This is the most practical way to optimize the contact patterns for both directions of rotation. However, this means that both tooth sides have to be found independently throughout the application of the LM algorithm.

Table 5 shows the estimated basic machine-tool settings for the pinion following the procedure described in Section 3. These estimated values allow us to establish the initial values for some variables in the LM algorithm. Other estimated basic data illustrated in Table 3 such as the curvature radius or the normal pressure angles fulfill the same requirement.

Table 6 shows the variables that are considered in the application of the LM algorithm to determine the machine-tool settings and cutter parameters of the closer concave tooth surface of the pinion to the reconstructed one. The initial values and their limits are illustrated as well in Table 6.

Table 5: Estimated basic machine-tool settings for the pinion.

Basic Machine-Tool Setting	Approach 1
Machine center to back, ΔX_{D1} [mm]	NA
Sliding base, ΔX_{B1} [mm]	NA
Blank offset, ΔE_{m1} [mm]	NA
Radial distance, S_{r1} [mm]	36.756
Cradle angle, q_1 [°]	59.104
Machine root angle, γ_{m1} [°]	41.199
Velocity ratio, m_{1c}	1.44671

NA: not available

At this stage of the research, an accurate value of the root cone angle is assumed to be obtained through some other methodology. This means that the machine root angle will be considered as known and equal to the value of the given design (41.767 deg.). On the other hand, the LM algorithm will be focused on the active tooth surface since a scarce information is provided by the point clouds at the fillet areas. This implies that the root fillet radius ρ_f is assumed, at this stage of the research, to be known and equal to the one provided in the given design (0.87 mm).

Table 6 shows as well the reached values of the machine-tool settings and cutter parameters when the optimization procedure is finished. They are reached after 109 iterations, achieving a minimum value in the objective function of $f(\mathbf{x}) = 9.24 \cdot 10^{-6}$ mm^2, a maximum positive deviation of 1.02 μm and a maximum negative deviation of -0.87 μm. Table 6 shows as well the values of the given design for a better comparison with the reached values.

Table 6: Initial data and results of the optimization of the concave tooth side of the pinion.

Variable	Fixed	Min.	Initial	Max.	Reached	Given Design
Machine center to back, ΔX_{D1} [mm]		-5.0	0.0	5.0	-1.936	-3.512
Sliding base, ΔX_{B1} [mm]		-5.0	0.0	5.0	0.088	1.471
Blank offset, ΔE_{m1} [mm]		-5.0	0.0	5.0	-1.336	1.218
Radial distance, S_{r1} [mm]		30.0	35.0	40.0	35.638	32.119
Cradle angle, q_1 [°]		50.0	55.0	60.0	50.0	52.454
Machine root angle, γ_{m1} [°]	✓					41.767
Swivel angle, j [°]	✓					0.0
Tilt angle, i [°]	✓					0.0
Velocity ratio, m_{1c}		1.0	1.5	2.0	1.4189	1.2746
Modified roll coef. C		-0.2	0.0	0.2	-0.0202	-0.0272
Modified roll coef. D		-0.2	0.0	0.2	-0.0002	0.0644
Cutter tip point radius, R_g [mm]		35.0	45.0	55.0	39.842	39.725
Blade pressure angle, α_{bl}		17.0	20.0	23.0	19.255	21.644
Root fillet radius, ρ_f [mm]	✓					0.87
Parabola coef., a_p [mm$^{(-1)}$]		0.0	0.001	0.002	0.001	0.0008
Point of tangency, u_o [mm]		2.5	3.0	3.5	3.0	3.031

A similar procedure is applied to determine the machine-tool settings and cutter parameters of the convex tooth surface of the pinion. Table 7 shows the initial and limit values of the variables,

and their reached values when the optimization process is finished. In this case, a total of 211 iterations were needed to reach a minimum value in the objective function of $f(\mathbf{x}) = 1.08 \cdot 10^{-5}$ mm^2, a maximum positive deviation of 1.06 μm and a maximum negative deviation of -1.26 μm.

Table 7: Initial data and results of the optimization of the convex tooth side of the pinion.

Variable	Fixed	Min.	Initial	Max.	Reached	Given Design
Machine center to back, ΔX_{D1} [mm]		-5.0	0.0	5.0	-0.801	0.525
Sliding base, ΔX_{B1} [mm]		-5.0	0.0	5.0	-0.692	-1.218
Blank offset, ΔE_{m1} [mm]		-5.0	0.0	5.0	2.230	0.631
Radial distance, S_{r1} [mm]		30.0	35.0	40.0	36.608	38.194
Cradle angle, q_1 [°]		45.0	55.0	65.0	45.0	56.547
Machine root angle, γ_{m1} [°]	✓					41.767
Swivel angle, j [°]	✓					0.0
Tilt angle, i [°]	✓					0.0
Velocity ratio, m_{1c}		1.0	1.5	2.0	1.4480	1.4893
Modified roll coef. C		-0.2	0.0	0.2	0.0274	0.0176
Modified roll coef. D		-0.2	0.0	0.2	-0.0005	-0.0139
Cutter tip point radius, R_g [mm]		35.0	45.0	55.0	48.164	47.860
Blade pressure angle, α_{br}		17.0	20.0	23.0	17.0	18.316
Root fillet radius, ρ_f [mm]	✓					0.87
Parabola coef., a_p [mm$^{(-1)}$]		0.0	0.001	0.002	0.0008	0.0008
Point of tangency, u_o [mm]		2.5	3.0	3.5	3.0	2.959

Figure 14 shows the deviations between the optimized tooth surfaces and the objective ones (the reconstructed tooth surfaces) of the pinion. The differences are under 2.5 μm.

6.6. Results of tooth contact and stress analyses

Figure 15 shows the results of tooth contact analysis when the optimized pinion tooth surfaces (derived in subsection 6.5) mesh with the estimated gear tooth surfaces following the approach 2* (derived in subsection 6.4). For both directions of rotation of the pinion, clockwise or counterclockwise, the user can foresee the designer's intent since a longitudinally oriented contact pattern can be visualized as in the given design (see Fig. 6). The location of the contact patterns on the tooth surfaces is not exactly the same as those observed in Fig. 6, since this type of contact pattern is very sensitive to changes in the geometry. Something similar occurs to the function of transmission errors where a concave down function is observed in Fig. 15, although the level of transmission errors is far from the expected value.

Figure 16 shows the evolution of the maximum contact pressure when the pinion rotates clockwise and the optimized convex tooth surface of the pinion is in mesh with the estimated concave tooth surface of the gear. The maximum level (about 1400 MPa) is very close to the maximum level observed in the given design (see Fig. 7(b)).

7. Conclusions

The performed research work allows the following conclusions to be drawn:

(1) A reverse engineering procedure for spiral bevel gears reconstructed from point clouds obtained with a non-contact metrology machine has been proposed.

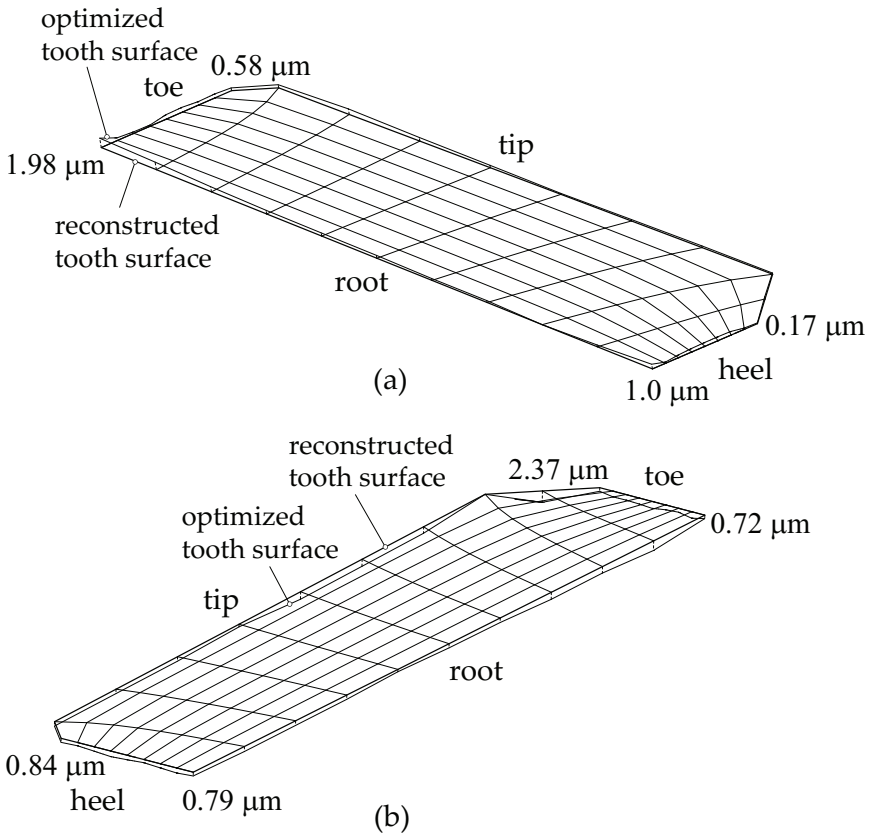

Figure 14: Geometry comparison between the reconstructed pinion tooth surfaces and the optimized ones at: (a) the concave tooth side (left side) and (b) the convex tooth side (right side).

(2) A methodology to derive the basic gear data from the reconstructed spiral bevel gear tooth surfaces has been developed. Among the basic gear data, the derivation of the outer transverse module allows the design torque of the gear drive to be estimated for finite element analysis.

(3) The basic machine-tool settings of the reconstructed gear have been estimated based on the derived basic gear data and compared with those of a given design. The results show that most of the basic machine-tool settings of the gear are well estimated, although an accurate estimate of the root cone angle is mandatory for an accurate determination of the sliding base and the machine root angle settings.

(4) A procedure to obtain the closer generated gear tooth surfaces of a spiral bevel pinion to the reconstructed ones have been proposed based on the application of the LM algorithm. For that purpose, a first estimation of the basic machine-tool settings of the reconstructed pinion has been performed. A good match between the optimized geometries and the reconstructed ones has been found.

(5) The results of tooth contact and stress analyses of the gear models obtained through the reverse engineering approach show that the designer's intent can be predicted up to a certain point. The direction of the contact pattern and the level of contact stresses can be well evaluated, although the level of transmission errors is still far from the expected value due to

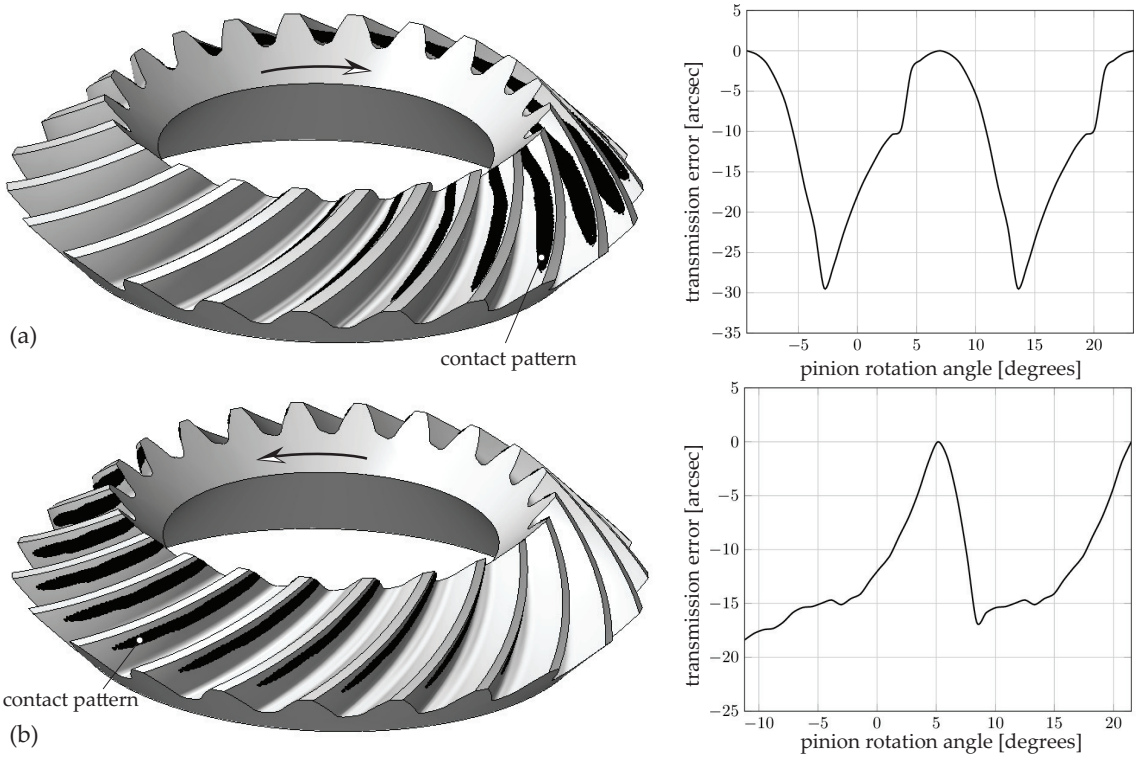

Figure 15: Results of tooth contact analysis between the optimized pinion tooth surfaces and the estimated gear tooth surfaces: (a) for a counterclockwise rotation of the pinion, and (b) for a clockwise rotation of the pinion.

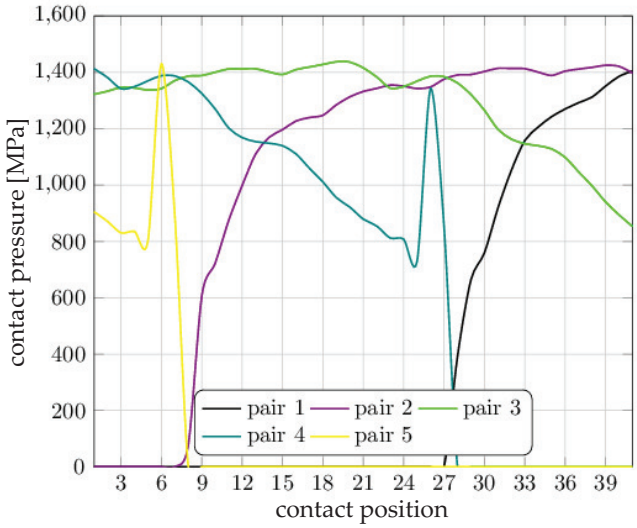

Figure 16: Contact pressure evolution when the optimized convex tooth surface of the pinion is in mesh with the estimated concave tooth surface of the gear during a clockwise rotation of the pinion.

the sensitivity of this function to irregularities on the gear tooth surfaces.

Acknowledgments

The authors express their deep gratitude to the Spanish Ministry of Economy, Industry and Competitiveness (MINECO), the Spanish State Research Agency (AEI) and the European Fund for Regional Development (FEDER) for the financial support of research project DPI2017-84677-P.

References

References

[1] T. Várady, R. R. Martin, J. Cox, Reverse engineering of geometric models - An introduction, CAD Computer Aided Design 29 (4) (1997) 255–268.

[2] S. H. Su, C. H. Tseng, Generating conjugate shapes using piecewise cubic spline functions, Computer Methods in Applied Mechanics and Engineering 187 (1-2) (2000) 245–260.

[3] X. Su, D. Houser, Alternative equation of meshing for worm-gear drives and its application to determining undercutting and reverse engineering, Journal of Mechanical Design 122 (June) (2000) 207–212.

[4] Q. Jiang, C. Gosselin, J. Masseth, Simulation of hypoid gear lapping, Journal of Mechanical Design, Transactions of the ASME 130 (11) (2008) 1126011–11260110.

[5] G. Liu, K. Chang, Z. Liu, Reverse engineering of machine-tool settings with modified roll for spiral bevel pinions, Chinese Journal of Mechanical Engineering (English Edition) 26 (3) (2013) 573–584.

[6] G. L. Liu, D. G. Li, L. Y. Wang, Reconstruction of real tooth surfaces of spiral bevel pinions with modified offset, Inverse Problems in Science and Engineering 23 (2) (2015) 214–234.

[7] C. Gosselin, Advanced Computer-Aided Gear Design , Analysis and Manufacturing, in: V. Goldfarb, E. Trubachev, N. Barmina (Eds.), New Approaches to Gear Design and Production, Mechanism and Machine Science, Vol. 81, Springer, 2020, pp.71–113.

[8] G. Goch, A. Günther, Areal gear flank description as a requirement for optical gear metrology, in: Towards Synthesis of Micro-/Nano-systems, 2006, pp. 47–52.

[9] Y. Peng, K. Ni, G. Goch, Areal evaluation of involute gear flanks with three- dimensional surface data, in: American Gear Manufacturers Association Fall Technical Meeting 2017, American Gear Manufacturers Association, 2017, pp. 106–119.

[10] A. Kumar, P. K. Jain, P. M. Pathak, Curve reconstruction of digitized surface using K-means algorithm, Procedia Engineering 69 (2014) 544–549.

[11] A. Fuentes-Aznar, I. Gonzalez-Perez, Integrating non-contact metrology in the process of analysis and simulation of gear drives, in: American Gear Manufacturers Association Fall Technical Meeting 2018, AGMA American Gear Manufacturers Association, 2018.

[12] I. Gonzalez-Perez, A. Fuentes-Aznar, Tooth contact analysis of cylindrical gears reconstructed from point clouds in: V. Goldfarb, E. Trubachev, N. Barmina (Eds.), New Approaches to Gear Design and Production, Mechanism and Machine Science, Vol. 81, Springer, 2020, pp. 219–237.

[13] I. Gonzalez-Perez, P. L. Guirao-Saura, A. Fuentes-Aznar, Application of the bilateral filter for the reconstruction of spiral bevel gear tooth surfaces from point clouds, Journal of Mechanical Design, Transactions of the ASME 143 (5) (2021) 1–10.

[14] H. Samet, Foundations of Multidimensional and Metric Data Structures, Morgan Kaufmann series in Computer Graphics and Geometric Modeling, Elsevier Science, 2006.

[15] L. Piegl, W. Tiller, The NURBS Book, Monographs in Visual Communication, Springer Berlin Heidelberg, 1996.

[16] American Gear Manufacturers Association, 2005. ANSI/AGMA 2005-C96, Design Manual of Bevel Gears. 1500 King Street, Suite 201, Alexandria, Virginia 22314.

[17] F. L. Litvin, A. Fuentes, Gear Geometry and Applied Theory, Cambridge University Press, 2004.

[18] Y. Jaluria, Computer Methods for Engineering, Taylor & Francis, New York, 1996.

[19] P. E. Gill, W. Murray, M. H. Wright, Practical Optimization, Academic Press, 1981.

[20] J. Nocedal, S. Wright, Numerical Optimization, Springer Series in Operations Research and Financial Engineering, Springer New York, 2000.

[21] G. I. Sheveleva, A. E. Volkov, V. I. Medvedev, Algorithms for analysis of meshing and contact of spiral bevel gears, Mechanism and Machine Theory 42 (2) (2007) 198–215.

[22] I. Gonzalez-Perez, A. Fuentes-Aznar, Implementation of a finite element model for gear stress analysis based on tie-surface constraints and its validation through the Hertz's theory, Journal of Mechanical Design, Transactions of the ASME 140 (2) (2018).

[23] Dassault Systemes: Abaqus/Standard Analysis User's Guide. Dassault Systemes Inc., Waltham, MA (2019).

[24] I. Gonzalez-Perez, A. Fuentes, K. Hayasaka, Analytical determination of basic machine-tool settings for generation of spiral bevel gears from blank data, Journal of Mechanical Design, Transactions of the ASME 132 (10) (2010).

[25] I. Gonzalez-Perez, A. Fuentes, R. Ruiz-Orzaez, An approach for determination of basic machine-tool settings from blank data in face-hobbed and face-milled hypoid gears, Journal of Mechanical Design, Transactions of the ASME 137 (9) (2015).